Development 138, 1925-1934 (2011) doi:10.1242/dev.060020


# Regulation of mammalian Notch signaling and embryonic development by the protein *O*-glucosyltransferase Rumi

**Rodrigo Fernandez-Valdivia[1], Hideyuki Takeuchi[2], Amin Samarghandi[1], Mario Lopez[1], Jessica Leonardi[3], Robert S. Haltiwanger[2] and Hamed Jafar-Nejad[1,3,4,5,6,*]**

## SUMMARY

Protein *O*-glucosylation is a conserved post-translational modification that occurs on epidermal growth factor-like (EGF) repeats harboring the $C^1$-X-S-X-P-$C^2$ consensus sequence. The *Drosophila* protein *O*-glucosyltransferase (Poglut) Rumi regulates Notch signaling, but the contribution of protein *O*-glucosylation to mammalian Notch signaling and embryonic development is not known. Here, we show that mouse *Rumi* encodes a Poglut, and that *Rumi*$^{-/-}$ mouse embryos die before embryonic day 9.5 with posterior axis truncation and severe defects in neural tube development, somitogenesis, cardiogenesis and vascular remodeling. Rumi knockdown in mouse cell lines results in cellular and molecular phenotypes of loss of Notch signaling without affecting Notch ligand binding. Biochemical, cell culture and cross-species transgenic experiments indicate that a decrease in Rumi levels results in reduced *O*-glucosylation of Notch EGF repeats, and that the enzymatic activity of Rumi is key to its regulatory role in the Notch pathway. Genetic interaction studies show that removing one copy of *Rumi* in a *Jag1*$^{+/-}$ (jagged 1) background results in severe bile duct morphogenesis defects. Altogether, our data indicate that addition of *O*-glucose to EGF repeats is essential for mouse embryonic development and Notch signaling, and that Jag1-induced signaling is sensitive to the gene dosage of the protein *O*-glucosyltransferase Rumi. Given that *Rumi*$^{-/-}$ embryos show more severe phenotypes compared to those displayed by other global regulators of canonical Notch signaling, Rumi is likely to have additional important targets during mammalian development.

**KEY WORDS: Notch signaling, *O*-glucosylation, Mouse, *Jag1*, EGF repeat, *Drosophila***

## INTRODUCTION

Notch signaling is one of the pathways widely used during animal development and in the adult maintenance of a variety of tissues and cell types (Fortini, 2009; Kopan and Ilagan, 2009). Mutations in several components of this pathway play causative roles in various diseases (Ellisen et al., 1991; Joutel et al., 1996; Bulman et al., 2000; Eldadah et al., 2001; Garg et al., 2005; Lee et al., 2009), including a multisystem developmental disorder called the Alagille syndrome (Li et al., 1997; Oda et al., 1997). The Notch proteins and their ligands are type I transmembrane proteins with a number of epidermal growth factor-like (EGF) repeats in their extracellular domain. EGF repeats usually consist of ~40 amino acids, including six cysteine residues that form three disulfide bonds to generate the three-dimensional structure of the EGF repeat (Harris and Spellman, 1993). Several forms of *O*-linked carbohydrates decorate the EGF repeats of *Drosophila* and mammalian Notch proteins (Moloney et al., 2000; Matsuura et al., 2008): *O*-fucose, *O*-GlcNAc (N-acetylglucosamine) and *O*-glucose. Loss of the enzyme responsible for the addition of *O*-fucose to Notch (protein *O*-fucosyltransferase 1) results in embryonic lethality, with phenotypes similar to a global loss of Notch signaling in flies and in mice (Okajima and Irvine, 2002; Sasamura et al., 2003; Shi and Stanley, 2003). Therefore, Notch signaling seems to be the primary biologically relevant target of Ofut1/Pofut1 during embryonic development.

*O*-glucosylation occurs on Notch and other proteins with EGF repeats harboring a $C^1$-X-S-X-P-$C^2$ consensus motif, where S is the glucosylated serine and $C^1$ and $C^2$ are the first and second cysteine residues in the target EGF repeat (Hase et al., 1988; Harris and Spellman, 1993). Vertebrate and *Drosophila* Notch proteins harbor the largest number of EGF repeats with predicted *O*-glucosylation motifs, although other proteins, including Notch ligands and several coagulation factors, also contain a number of such motifs (Moloney et al., 2000). Mutations in *Drosophila rumi*, which encodes the fly protein *O*-glucosyltransferase, result in a temperature-sensitive loss of Notch signaling (Acar et al., 2008). Moreover, RNAi-mediated knockdown of Rumi in *Drosophila* S2 cells causes a severe reduction in the level of *O*-glucose on Notch EGF repeats. These observations established an important role for protein *O*-glucosylation in the regulation of *Drosophila* Notch signaling (Acar et al., 2008).

The glycosyltransferase activity of fly Rumi is mediated by the CAP10 domain, which is named after the cryptococcal protein CAP10 (Chang and Kwon-Chung, 1999). To examine whether the role of Rumi in the regulation of Notch signaling is conserved

[1]Brown Foundation Institute of Molecular Medicine (IMM), The University of Texas Health Science Center, Houston, TX 77030, USA. [2]Department of Biochemistry and Cell Biology, Institute for Cell and Developmental Biology, Stony Brook University, Stony Brook, NY 11794, USA. [3]Program in Developmental Biology, Baylor College of Medicine, Houston, TX 77030, USA. [4]Department of Biochemistry and Molecular Biology, Medical School, The University of Texas Health Science Center, Houston, TX 77030, USA. [5]Program in Genes and Development, The University of Texas Graduate School of Biomedical Sciences, Houston, TX 77030, USA. [6]Program in Biochemistry and Molecular Biology, The University of Texas Graduate School of Biomedical Sciences, Houston, TX 77030, USA.

*Author for correspondence (hamed.jafar-nejad@uth.tmc.edu)

**Accepted 18 February 2011**

between flies and mammals, we initiated genetic, cell culture and biochemical studies on mouse genes encoding CAP10-containing proteins and found that only one of these homologs, mouse Rumi, has Poglut activity. Our data indicate that *Rumi* is required for embryonic development and Notch signaling in the mouse. Our data further suggest that Jag1-induced Notch signaling is sensitive to the gene dosage of mouse *Rumi*.

## MATERIALS AND METHODS

### Generation of the *Rumi* mutant mouse

The IST10323G11 (Texas A&M Institute for Genomic Medicine) (Hansen et al., 2008) heterozygous C57BL/6N ES cell clone with a gene trap insertion in intron 2 of *Rumi* was used to generate the *Rumi* mutant mouse (official name: $Poglut1^{GT(IST10323G11)TIGM}$). For Southern blot analysis, genomic DNA was digested with *Avr*II, *Bgl*II or *Hin*dIII, and the blots were hybridized with a probe against the neomycin resistance gene (Fernandez-Valdivia et al., 2010). All mice were housed in temperature-controlled (22±2°C) rooms, with 12 hour light, 12 hour dark photocycle, and fed with rodent chow meal and fresh water, ad libitum. All surgical procedures as well as euthanasia protocols were approved by the Animal Welfare Committee of The University of Texas Health Science Center at Houston, and were in accordance with the procedures outlined in the 'Guide for the Care and Use of Laboratory Animals' (NIH publication 85-23).

### Genotyping

Genomic DNA from tail tips, yolk sacs or ES cells was used for PCR genotyping. Paraformaldehyde-fixed early embryos were directly genotyped after immunohistochemical experiments. For primers, see Table S1 in the supplementary material.

### Embryonic studies

Embryos were collected between E7.5 and E10.5. E8.0 embryos were fixed in 4% PFA in PBS, washed with PBS and pre-embedded in 1% low melting point agarose in PBS. Agarose blocks were dehydrated with alcohol series, cleared with xylenes and embedded in paraffin blocks. Embryo blocks were sectioned at 5 μm, and the sections stained with Hematoxylin and Eosin.

### DBA lectin histochemistry and immunohistochemistry

DBA lectin histochemistry and Pecam1 staining were performed as described previously (McCright et al., 2002; Kuhnert et al., 2005). For Rumi staining, antigen was retrieved in a boiling solution of 10 mM sodium citrate (pH 6.0) for 20 minutes. The anti-Rumi antibody was raised in rabbits against the peptide RQKDSGSKWKVFLD (see Fig. S2 in the supplementary material). Anti-Rumi and Cy3-conjugated goat anti-Rabbit secondary (Jackson ImmunoResearch Laboratories) antibodies were used at 1:250.

### RT-PCR and qRT-PCR analysis

Total RNA was extracted using QIAzol and RNeasy kit (Qiagen). qRT-PCR was performed using 100 ng total RNA per well and TaqMan One-Step RT-PCR Master Mix (Applied Biosystems). Relative mRNA levels were compared using the $2^{-\Delta\Delta CT}$ method, with *18S* as control. For *Hes1* qRT-PCR in Neuro2A cells, 2 μg of total RNA per well were used. For RT-PCR, 1 μg of total RNA per lane was used to synthesize cDNA. For primers and primers/probe sets see Table S1 in the supplementary material.

### Cell culture, Rumi knockdown, immunoblots and biotinylation assays

NMuLi, HepG2, BNL-CL2, Neuro2A, HEK293T and C2C12 cells were cultured in DMEM (Thermo Fisher) supplemented with 10% FBS (Thermo Fisher). Transfections were performed in OPTI-MEM (Invitrogen), using either Fugene HD (Roche) or Lipofectamine 2000 (Invitrogen). pLKO.1 plasmids (Moffat et al., 2006) encoding shRNA-30 against mouse *Rumi* and non-target control shRNA-NT (Sigma) were used to generate stably transfected cells. Plasmids used for transient transfection include: mouse *Rumi* cDNA (pcDNA4-mRumi); EGFP-C2 (Clontech); pTracer; pTracer-hRumi-FLAG; and pTracer-hRumi-FLAG-G169E mutant. Antibodies used in western blots are anti-mouse Rumi (1:500, this study), anti-α-Tubulin (1:2000, Santa Cruz Biotechnology), anti-GFP (1:4000, Abcam), anti-β-Actin-HRP (1:2000, Santa Cruz Biotechnology), anti-β-Actin (1:2000, Abcam) and anti-cleaved Notch1 (Val1744, 1:1000, Cell Signaling Technology). Biotinylation assays were performed as described previously (Mumm et al., 2000; Rampal et al., 2005) using the anti-Notch1 $N_a$ polyclonal antibody (Lu and Lux, 1996).

### Flow cytometry

Flow cytometry was performed on a BD FACS Aria II according to published protocols with slight modifications (Yang et al., 2005; Stahl et al., 2008). Purified rat Dll1-human Fc (1 μg/ml), rat Jag1-human Fc (0.5 μg/ml) (Hicks et al., 2000) and human Fc (1 μg/ml) were preclustered with R-PE conjugated anti-human Fc for 1 hour at 4°C. The following antibodies were used: anti-Notch1 (10 μg/ml, R&D Systems); R-PE-conjugated F(ab')2 anti-sheep IgG (1:100), sheep IgG (10 μg/ml), human Fc fragment (1 μg/ml) and R-PE-conjugated F(ab')2 anti-human Fc fragment (1:100) from Jackson ImmunoResearch Laboratories.

### Differentiation assays on Neuro2A cells

Neuro2A differentiation assays were performed as described previously (Franklin et al., 1999) with some modifications. At least three independent experiments were performed for each cell line/transfection. In each experiment, five independent fields of ~100 cells were used for quantification of the neurite extension per cell line/transfection.

### Transgenic fly experiments

The ORF of the rat Jag1 was cloned into the *pUAST-attB* vector and integrated into the fly genome as described (Venken et al., 2006; Bischof et al., 2007). *UAS-ratDLL1-HA*, *UAS-mDLL3-FLAG* (Geffers et al., 2007) and *UAS-attB-ratJagged1* (this study) were used to overexpress mammalian ligands in mitotic clones of the null allele $rumi^{\Delta 26}$ (Acar et al., 2008) or in mitotic clones of a wild-type chromosome (control) by using the MARCM technique (Lee and Luo, 2001) as described previously (Acar et al., 2008). Wing imaginal discs were dissected and fixed by using standard protocols and stained with α-Jag1 (1:100, Santa Cruz Biotechnology), α-Cut (1:500, DSHB) and/or α-FLAG (1:500, Sigma) antibodies.

### Enzymatic assays

Cells and livers were homogenized in approximately 5 volumes of TBS-Complete, and incubated on ice for 60 minutes. After centrifugation, the supernatants were used as protein extracts. Enzymatic assays for hRumi-FLAG and hRumi-G169E-FLAG were performed on cell lysates from transiently transfected HEK293T cells. Both *O*-glucosyltransferase and *O*-fucosyltransferase 1 assays were performed as previously described (Shao et al., 2002) with slight modifications.

### Mass spectrometric analysis

A cDNA encoding a region of the extracellular domain of mouse Notch2 encompassing EGF repeats 13-18 (amino acids 468-699) was inserted into pSecTag2/Hygro C vector (Invitrogen) so that the protein was expressed with a C-terminal Myc-6xHis tag. The expression vector was transiently transfected into C2C12-NT and C2C12-30 cells using PEI. Proteins were purified from the culture medium by Ni-NTA agarose affinity chromatography (Qiagen). Equivalent amounts of proteins from each cell line were separated by Nu-PAGE gradient gel (4-12%, Invitrogen), detected using a zinc-stain (BioRad), and bands were cut out and digested with Asp-N protease (Sigma) at 37°C for 16 hours as described (Nita-Lazar and Haltiwanger, 2006). The resulting (glyco)peptides were purified by Zip-Tip (Millipore) and analyzed by nanoLC-MS/MS on an Agilent XCT Ultra ion trap mass spectrometer with a CHIP-Cube interface as described (Leonhard-Melief and Haltiwanger, 2010). The relative quantities of the (glyco)peptides were analyzed by differential MS approach using the extracted ion chromatograms of each ion (Acar et al., 2008).

### Statistics

Data are shown as mean±s.e.m. *P* values were determined by Student's *t*-test or one-way ANOVA. For Neuro2A differentiation assays, one-way ANOVA was used to compare all groups to Neuro2A-NT, with Dunnet error protection at a 95% confidence interval.

## RESULTS

### Rumi is the sole enzyme in the mouse capable of adding *O*-glucose to EGF repeats

*Drosophila* Rumi has three homologs in mammals: Rumi [also known as CAP10-like protein 46 kDa (CLP46) and KTEL-containing 1 (KTELC1)], KDEL-containing 1 (KDELC1) and KDELC2 (Fig. 1A). Among these three proteins, mouse Rumi shares the highest homology with fly Rumi (56% overall identity; 66% identity in the CAP10 domain). The enzymatic and physiological roles of these proteins have not been reported (Kimata et al., 2000; Teng et al., 2006). Biochemical analysis and cross-species overexpression studies in flies indicate that the mouse/human Rumi is the only Drosophila Rumi homolog with similar enzymatic and functional characteristics (H.T., R.F.-V., H.J.-N. and R.S.H., unpublished). Therefore, we injected ES cells with gene-trapped *Rumi* alleles showing ~50% decrease in *Rumi* mRNA expression (Fig. 1C; see Fig. S1 in the supplementary material) into blastocysts and established a *Rumi* mutant mouse strain (here referred to as $Rumi^{-}$ or $Rumi^{\beta Geo}$ allele) from ES cell line IST10323G11. PCR sequencing and Southern blot with a *Neo* probe on genomic DNA confirmed a single gene trap insertion in intron 2 of the *Rumi* gene (Fig. 1B,D,E). qRT-PCR assays on P0 liver extracts of $Rumi^{+/-}$ newborns showed a 50% decrease in *Rumi* mRNA levels compared with wild-type littermates, demonstrating that the gene trap efficiently blocks the expression of *Rumi* mRNA (Fig. 2A). Moreover, immunostaining with a polyclonal anti-Rumi antibody (see Fig. S2 in the supplementary material) shows broad expression in wild-type and $Rumi^{+/-}$ embryos but no expression in $Rumi^{-/-}$ embryos (Fig. 2B,C; data not shown). We conclude that this allele in either null or a strong hypomorph.

To assess whether a decrease in Rumi levels affects the protein *O*-glucosyltransferase (Poglut) activity of mouse tissue extracts towards EGF repeats, we performed Poglut assays on liver extracts from newborn $Rumi^{+/-}$ animals and their wild-type littermates. We find that loss of one copy of *Rumi* results in ~50% decrease in the Poglut activity but no significant change in Pofut1 activity (Fig. 2D), indicating that the effect observed on Poglut activity in $Rumi^{+/-}$ animals is specific. RT-PCR assays show that the other two mammalian homologs of *Drosophila* Rumi – *Kdelc1* and *Kdelc2* – are co-expressed with *Rumi* in neonatal mouse livers and in several mammalian liver cell lines (Fig. 2E). qRT-PCR on liver extracts indicates that *Kdelc1/Kdelc2* mRNA are expressed at moderate levels but do not change in $Rumi^{+/-}$ compared with controls (Fig. 2A). Therefore, we conclude that these two proteins are not able to compensate for the loss of one copy of *Rumi* in the neonatal liver. Western blot analysis using our polyclonal anti-Rumi antibody indicates that Rumi is broadly expressed in neonatal and adult mouse tissues (Fig. 2F), in agreement with previous reports on the broad distribution of Poglut activity in rat tissues (Shao et al., 2002) and human *Rumi* mRNA in adult human tissues (Teng et al., 2006). Altogether, these data indicate that Rumi is the only Poglut enzyme in the mouse liver (and likely other tissues) able to add an *O*-linked glucose residue to EGF repeats with a $C^1$-X-S-X-P-$C^2$ consensus motif.

### Early embryonic lethality and severe cardiovascular defects in embryos lacking Rumi

$Rumi^{+/-}$ animals are viable and fertile, and do not exhibit gross developmental abnormalities. From $Rumi^{+/-}$ intercrosses, wild-type and $Rumi^{+/-}$ heterozygous P0 progeny were obtained at a Mendelian ratio, but no newborn $Rumi^{-/-}$ mutants were obtained (Table 1). This observation suggests that *Rumi* is essential for mouse embryonic development. We therefore set timed pregnancies to study the embryonic phenotypes of $Rumi^{-/-}$ embryos. At E7.0-E7.5, $Rumi^{-/-}$ embryos could not be morphologically distinguished from their heterozygous and wild-type littermates (not shown). At E8.0, $Rumi^{-/-}$ embryos are characterized by an abnormally expanded neural plate that does not fold properly (Fig. 3C,F; compare with Fig. 3A,B,D,E), absence of heart rudiments (Fig. 3C) and posterior axis truncation. Despite their abnormal morphology, $Rumi^{-/-}$ embryos form the three embryonic germ layers (Fig. 3I; compare with Fig. 3G,H) and an allantois (Fig. 3C). A normal amniotic membrane (a), with its mesodermal and ectodermal components, is present in $Rumi^{-/-}$ embryos (Fig. 3F,I). In $Rumi^{-/-}$ embryos, the anterior ectoderm is expanded and disorganized, especially towards the midline, and the amount of mesodermal tissues seems decreased compared with wild-type and heterozygous embryos (Fig. 3G-I). However, a monolayer of definitive endoderm is present in the ventral side of $Rumi^{-/-}$ embryos, similar to wild-type and heterozygous embryos (Fig. 3G-I). At this stage, somites were observed in wild-type and heterozygous

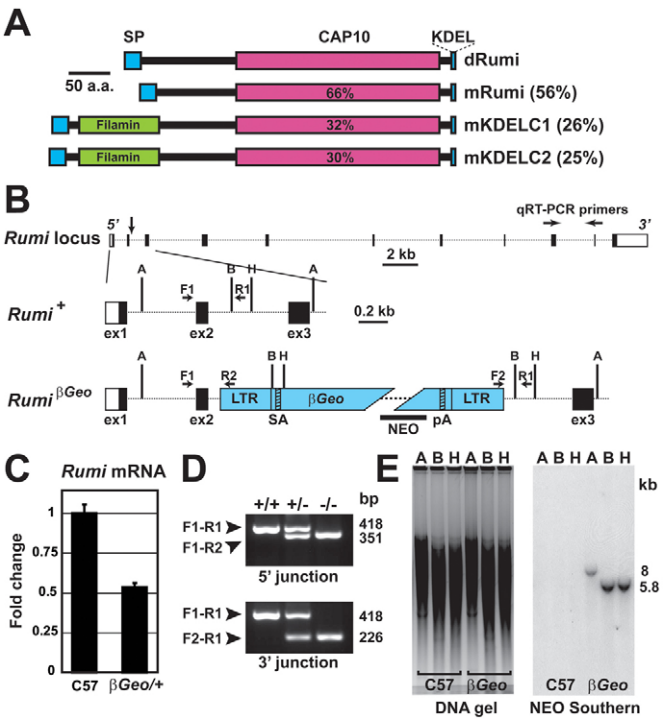


**Fig. 1. Generation of a loss-of-function allele of mouse *Rumi*.** (**A**) Structure of the mouse CAP10 proteins and their amino acid identity to *Drosophila* Rumi (dRumi). Blue boxes at N and C termini indicate the signal peptide and the ER-recycling signal, respectively. (**B**) The top panel shows the structure of the mouse *Rumi* locus. The vertical arrow shows the insertion site of the gene trap in intron 2 (ex, exon; SA, splice acceptor; pA, polyAdenylation signal; LTR, long terminal repeat; NEO, neomycin resistance gene probe). *Avr*II (A), *Bgl*II (B) and *Hind*III (H) sites are depicted by vertical lines. (**C**) qRT-PCR on RNA extracted from wild-type C57BL6 (C57) and the $Rumi^{\beta Geo/+}$ ES cell IST10323G11. Data are mean±s.e.m. (**D**) Multiplex PCR genotyping on genomic DNA with primers F1, R1 and R2 (5′ junction) and F1, R1 and F2 (3′ junction). (**E**) Southern blot analysis with the NEO probe to verify unique insertion of the 6.5 kb VICTR76 gene trap vector in the *Rumi* locus. Insertion of the gene trap vector in *Rumi* results in a unique 8.0 kb band upon digestion with *Avr*II (A). *Bgl*II (B) and *Hind*III (H) digestions each release a unique fragment of ~5.8 kb from the mutant *Rumi* allele. Note the comparable amounts of digested genomic DNA loaded for C57 and $Rumi^{\beta Geo/+}$ genotypes.

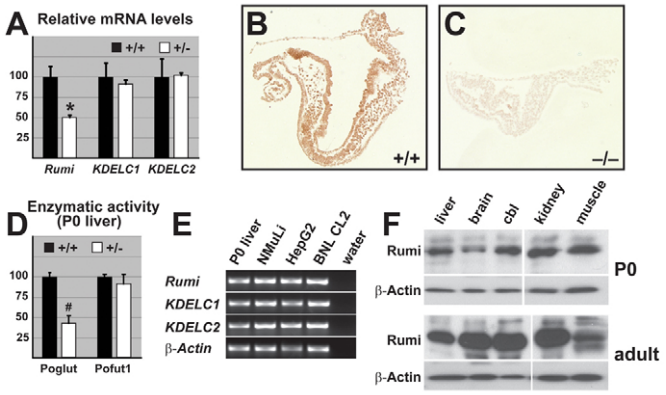


**Fig. 2. Rumi is the primary Poglut in the mouse.** (**A**) qRT-PCR for *Rumi*, *Kdelc1* and *Kdelc2* on neonatal liver extracts from *Rumi*$^{+/-}$ and *Rumi*$^{+/+}$. *$P$=0.003. Data are mean±s.e.m. The ranges of Ct values in the wild-type liver are 26.7-27.3 (*Rumi*), 28.2-29.0 (*Kdelc1*) and 27.0-28.1 (*Kdelc2*). (**B**,**C**) Sagittal section of E8.0 *Rumi*$^{+/+}$ and *Rumi*$^{-/-}$ embryos stained with anti-Rumi antibody. Identical staining protocol and image acquisition and processing parameters were used for both genotypes. (**D**) Poglut and Pofut1 enzymatic assays on the neonatal liver extracts from *Rumi*$^{+/-}$ and *Rumi*$^{+/+}$ mice. #$P$<0.002. Data are mean±s.e.m. (**E**) RT-PCR assays on neonatal mouse liver and cell lines derived from human hepatocellular carcinoma (HepG2), and from adult (NMuLi) and embryonic (BNL CL2) mouse liver. (**F**) Western blot analysis shows that Rumi is broadly expressed in the newborn and adult mouse tissues. cbl, cerebellum.

embryos (Fig. 3J,K), but not in *Rumi*$^{-/-}$ embryos (Fig. 3L). At E8.5, *Rumi*$^{-/-}$ embryos showed a neural plate that fails to fold properly, but continues to expand in the anterior part of the embryo (arrow in Fig. 3O; compare with Fig. 3M,N). In addition, the posterior parts of the embryo are completely lacking, and the allantois (bracket in Fig. 3O) is directly connected to the anterior embryonic structures. At this stage, we still did not observe any somites or heart formation in *Rumi*$^{-/-}$ embryos ($n$=28). At E9.5, most *Rumi*$^{-/-}$ embryos started to show signs of resorption, all of them were unturned and exhibited severe growth retardation, and the neural plate remained unfolded (Fig. 3R; compare with Fig. 3P,Q). By E10.5, all *Rumi*$^{-/-}$ embryos were in resorption and the number of homozygous mutants was already less than that expected from the Mendelian ratio, indicating that some embryos were fully resorbed at this developmental stage (Table 1). Therefore, *Rumi*$^{-/-}$ mutants die at or before E9.5, with phenotypes more severe than animals proposed to disrupt canonical Notch signaling like double mutant for presenilin 1 and presenilin 2 (Donoviel et al., 1999), *Rbpj* (Oka et al., 1995) or *Pofut1* (Shi and Stanley, 2003), suggesting that proteins other than the Notch pathway components might also depend on Rumi for their function (see Table S2 in the supplementary material).

As cardiovascular phenotypes are one of the hallmarks of Notch pathway mutant phenotypes in mice (Krebs et al., 2000; Shi and Stanley, 2003; Roca and Adams, 2007), we analyzed the cardiovascular development in embryos and yolk sacs between E8.5 to E9.5. Pecam1 staining showed severe cardiovascular defects in E8.5 *Rumi*$^{-/-}$ embryos, characterized by abnormal vascularization, absence of dorsal aorta and intersomitic vasculature, and cardia bifida (arrowheads indicate unfused cardiogenic plates in Fig. 4C,F; compare with Fig. 4A,B,D,E). At this stage, no Pecam1 staining was observed on the dorsal side of the head structures (Fig. 4F). At E9.5, disorganized vascular networks were present on the dorsal side of the head in some embryos (Fig. 4I; compare with Fig. 4G,H), indicating

**Table 1. *Rumi* homozygous mutants show embryonic lethality**

| | E7.5 | E8.5 | E9.5 | E10.5 | P0 |
|---|---|---|---|---|---|
| Litters | 2 | 13 | 8 | 4 | 3 |
| Pups | 18 | 108 | 62 | 41 | 16 |
| *Rumi*$^{+/+}$ | 4 | 28 | 13 | 14 | 6 |
| *Rumi*$^{+/-}$ | 10 | 52 | 33 | 20 | 10 |
| *Rumi*$^{-/-}$ | 4 | 28 | 16 | 7 | 0 |

*Rumi*$^{+/-}$ mice intercrosses show that whereas *Rumi*$^{+/+}$ and *Rumi*$^{+/-}$ animals were born at a Mendelian ratio at birth (P0), no *Rumi*$^{-/-}$ could be identified. Between E7.5 and E9.5 *Rumi*$^{+/+}$, *Rumi*$^{+/-}$ and *Rumi*$^{-/-}$ could be found at a Mendelian ratio, although at E9.5 most *Rumi*$^{-/-}$ embryos were in the process of resorption. At E10.5, all *Rumi*$^{-/-}$ embryos were in resorption, and their number was less than that expected from the Mendelian ratio.

that vascular development continued beyond E8.5, albeit in an abnormal manner. At E9.5, *Rumi*$^{-/-}$ embryos showed no heart, and the cardiogenic plates were still unfused (Fig. 4I). Whole-mount staining of the yolk sacs with anti-Pecam1 showed severe vascular remodeling defects in *Rumi*$^{-/-}$ at E8.75. *Rumi*$^{-/-}$ yolk sacs contained large blood sinusoids (Fig. 4L) instead of the normal vascular trees observed in wild-type and heterozygous yolk sacs (Figs 4J,K). In wild-type and *Rumi*$^{+/-}$ animals, Pecam1 staining of yolk sac sections at E8.75 shows a characteristic membrane staining of endothelial cells (Fig. 4M,N,P,Q). By contrast, *Rumi*$^{-/-}$ yolk sacs show a diffuse staining for Pecam1 and a lack of endothelial remodeling (Fig. 4O,R). Defects in vascular remodeling and dorsal aorta formation are reported in various mutant backgrounds affecting the Notch signaling pathway (Krebs et al., 2000; Shi and Stanley, 2003; Roca and Adams, 2007). Given the severe growth retardation of *Rumi*$^{-/-}$ embryos, it is difficult to ascertain that the only cause of the observed vascular defects is indeed loss of Notch signaling.

## Rumi modulates the Notch signaling pathway in mouse cell lines

Activation of Notch signaling results in decreased number and length of neurites extended from the Neuro2A mouse neuroblastoma cells, whereas inhibiting Notch signaling causes an increase in the number, length and the branching of neurites in these cells (Franklin et al., 1999; Mishra-Gorur et al., 2002; Ishikura et al., 2005). To test whether downregulation of endogenous Rumi affects Notch signaling and neurite extension, we established Neuro2A cells stably transfected with shRNA-30 – which efficiently knocks down Rumi and decreases the Poglut activity in mouse cell lines (Fig. 5A,B; see Fig. S2 in the supplementary material) – or the control shRNA-NT. qRT-PCR assays show an 89.6% decrease in *Hes1* transcript levels in Neuro2A-30 cells compared with the Neuro2A-NT cells (Fig. 5A). Differentiation assays show that after 4 hours in differentiation medium, there is a dramatic increase in the number and the length of neurites upon Rumi knockdown (Fig. 5C,D). Quantification of results from several independent differentiation assays indicates that ~45% of Rumi-knockdown Neuro2A cells harbor extensions longer than one cell diameter after 16-20 hours of differentiation (Fig. 5F,K). Only ~13% of control cells had such extensions (Fig. 5E,K). These results strongly suggest that Rumi regulates Notch signaling and neurite extension in Neuro2A cells.

To ensure that the effects observed in Neuro2A-30 cells are not due to off-target effects, we asked whether human Rumi (hRumi) – which is not affected by shRNA-30 (not shown) – can rescue the neurite phenotypes caused by mouse Rumi (mRumi) knockdown. We find that hRumi-FLAG, but not the empty vector, can rescue the increased neurite extension phenotype caused by shRNA-30 (Fig. 5G,H,K). To address whether Rumi plays a non-enzymatic role in mammalian cells, we overexpressed hRumi-G169E-FLAG,

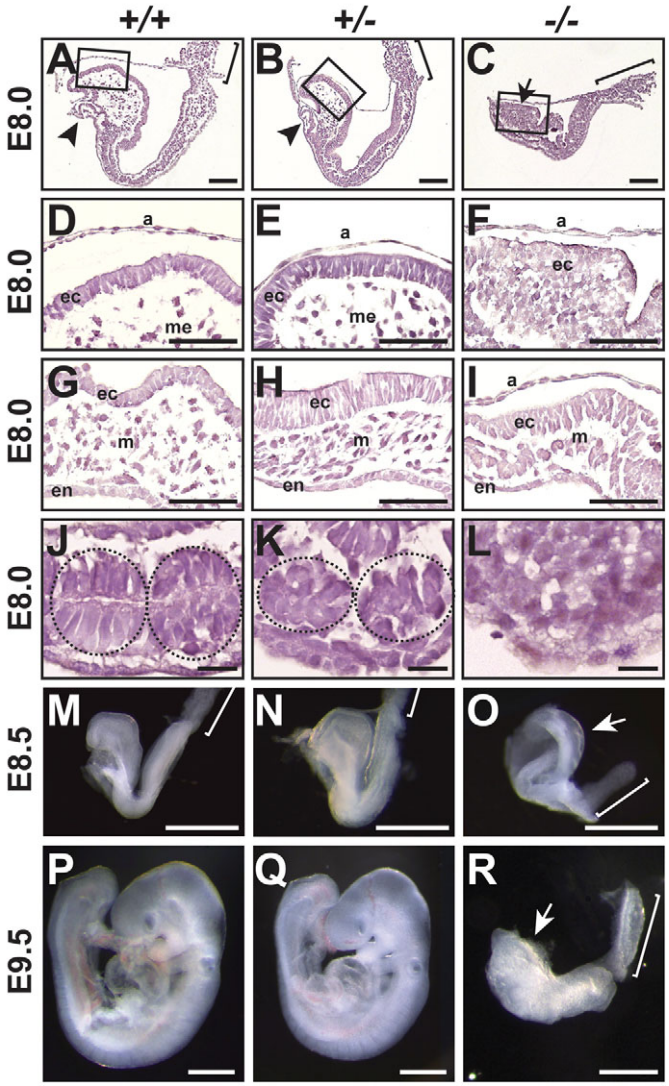


**Fig. 3. Loss of *Rumi* results in severe growth retardation and multiple abnormalities in mouse embryos.** (A-L) Hematoxylin and Eosin staining of sagittal sections of E8.0 embryos. (**A-F**) At E8.0, *Rumi*$^{-/-}$ embryos display expansion of the dorsal anterior structures (arrow), absence of cardiac rudiments (arrowhead in A,B) and axis shortening/truncation. However, the allantois (brackets in A-C,M-O,R) is present in mutant embryos (C). Scale bars: 100 μm. D-F are higher magnification of the boxed areas in A-C. Whereas wild-type (D) and heterozygous (E) embryos display normal organization of the neural ectoderm (ec) and cephalic mesenchyme (me), *Rumi*$^{-/-}$ embryos (F) show a disorganized ectoderm (ec). A normal, bilayered amniotic membrane (a) is present in *Rumi*$^{-/-}$ embryos. Scale bars: 50 μm. (**G-I**) Sections from the anterior region of E8.0 embryos. *Rumi*$^{-/-}$ embryos (I) do form ectoderm (ec), mesoderm (m) and endoderm (en) layers, but the amount of mesodermal tissue seems to be reduced. As the amniotic cavity of *Rumi*$^{-/-}$ embryos is smaller than their wild-type and heterozygous counterparts, the amniotic membrane (a) is visible in the *Rumi*$^{-/-}$ embryo section (I). Scale bars: 50 μm. (**J-L**) Somites (dashed ovals) can be seen in sagittal sections of E8.0 wild-type (J) and heterozygous (K) embryos, but not in *Rumi*$^{-/-}$ embryos (L). Scale bars: 20 μm. (**M-O**) At E8.5, *Rumi*$^{-/-}$ embryos exhibit an unfolded neural plate (arrow in O) and posterior axis truncation, with an allantois directly connected to the anterior structures. Scale bars: 500 μm. (**P-R**) At E9.5, *Rumi*$^{-/-}$ embryos exhibit severe growth retardation and a neural tube that remains unfolded (arrow in R). Scale bars: 500 μm. (M-R) Lateral views.

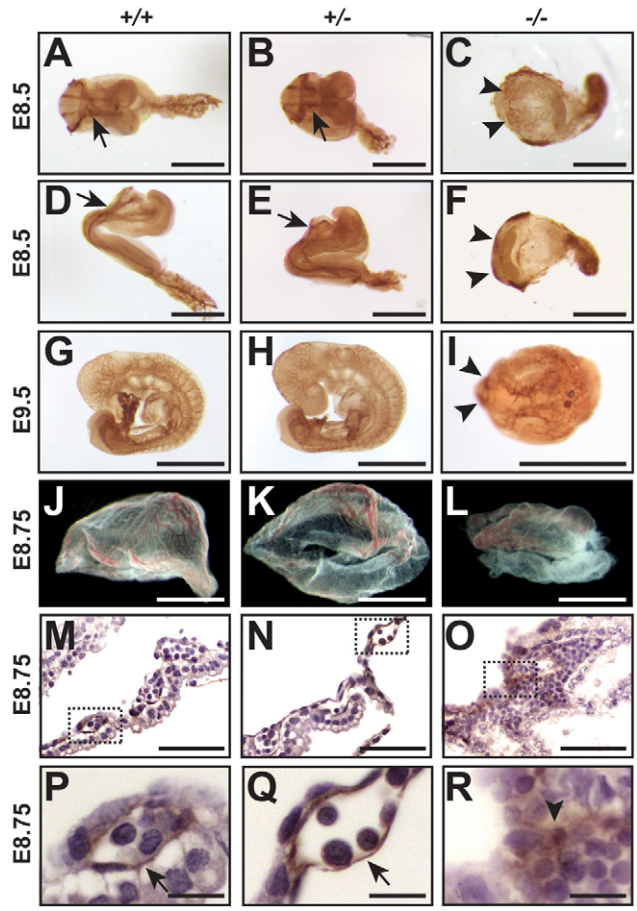


**Fig. 4. Pecam1 staining reveals severe cardiovascular defects in *Rumi* mutant embryos.** (A-I) Pecam1 staining of embryos and yolk sacs. (**A-F**) At E8.5, *Rumi*$^{-/-}$ embryos show cardia bifida, characterized by unfused cardiogenic plates (arrowheads) and absence of dorsal aorta. C and F are ventral and dorsal views of the same embryo, respectively. The heart is indicated by an arrow in A,B,D,E. Scale bars: 500 μm. (**G-I**) At E9.5, *Rumi*$^{-/-}$ embryos show no heart, with the cardiogenic plates still unfused (arrowheads) and severely abnormal vascularization. (I) Dorsal view. Scale bars: 1 mm. (**J-L**) At E8.75, *Rumi*$^{-/-}$ yolk sacs show abnormal vascular remodeling, characterized by the presence of several blood sinusoids. Scale bars: 1 mm. (**M-R**) Pecam1 staining of E8.75 yolk sacs marks the endothelial cells (arrows) in wild-type (P) and heterozygous (Q) animals. Note the diffused Pecam1 staining and absence of endothelial remodeling (arrowhead in R) in *Rumi*$^{-/-}$ animals. Scale bars: 50 μm. P-R are high magnification views of boxed areas in M-O. Scale bars: 10 μm.

which is enzymatically inactive (Fig. 5J), in Neuro2A-30 cells. hRumi-G169E-FLAG is not able to rescue the neurite outgrowth phenotype in Neuro2A-30 cells (Fig. 5I,K), even though hRumi-FLAG and hRumi-G169E-FLAG are expressed at comparable levels upon transient transfection (see Fig. S3 in the supplementary material). Altogether, these observations indicate that a decrease in the Poglut activity caused by mRumi knockdown significantly promotes neurite extension in Neuro2A cells, most probably owing to a decrease in Notch signaling.

We also assessed the effects of Rumi knockdown on Notch *O*-glucosylation and signaling in the C2C12 mouse myoblast cells. Stable transfection of C2C12 cells with shRNA-30 results in a 90% decrease in Poglut activity compared with control cells (Fig. 6A),

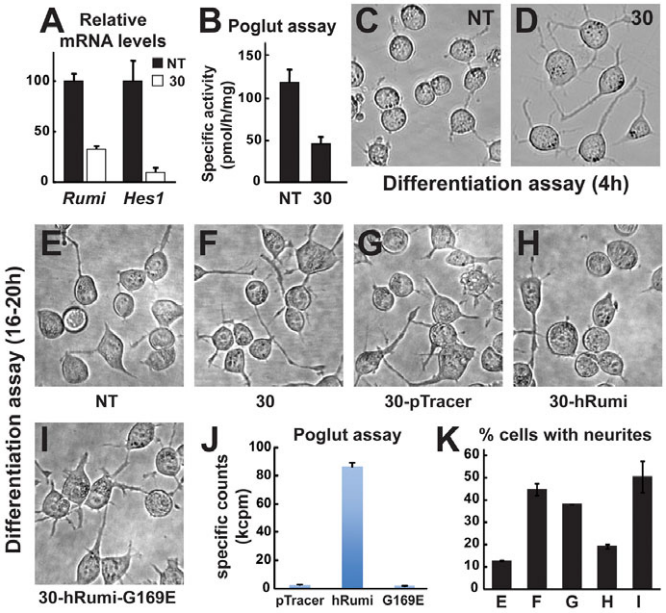


**Fig. 5. Rumi knockdown promotes neurite extension in the Neuro2A neuroblastoma cell line.** (**A**) qRT-PCR assays show a ~67% decrease in *Rumi* transcript levels ($P$=0.0006) and an 89.6% decrease in *Hes1* levels ($P$=0.0016) in Neuro2A-30 cells compared with that in the Neuro2A-NT cells. (**B**) Poglut assays show a ~65% decrease in the enzymatic activity of Neuro2A-30 cells compared with Neuro2A-NT cells. Data in A,B are mean±s.e.m. (**C**,**D**) Differentiation assays at 4 hours on Neuro2A-NT and Neuro2A-30 cells. (**E-I**) Differentiation assays at 16-20 hours on Neuro2A-NT (E), Neuro2A-30 (F) and Neuro2A-30 cells transiently transfected with pTracer empty vector (G), pTracer-hRumi-FLAG (H) and pTracer-hRumi-G169E-FLAG (I). (**J**) Poglut assays indicate that hRumi-G169E-FLAG is enzymatically inactive. (**K**) Percentage of cells bearing neurites longer than one cell diameter after 16-20 hours of differentiation. Letters on the *x*-axis show the data for the corresponding panels. One-way ANOVA indicates that (E) is significantly different from all others except for (H) ($P$<0.0001). *t*-test indicates that the percentage of cells with neurites in Neuro2A-30 (F) is significantly different from Neuro2A-30-hRumi (H) ($P$=0.0008), but not from Neuro2A-30-G169E cells (I) ($P$=0.49). Data in J,K are mean±s.e.m.

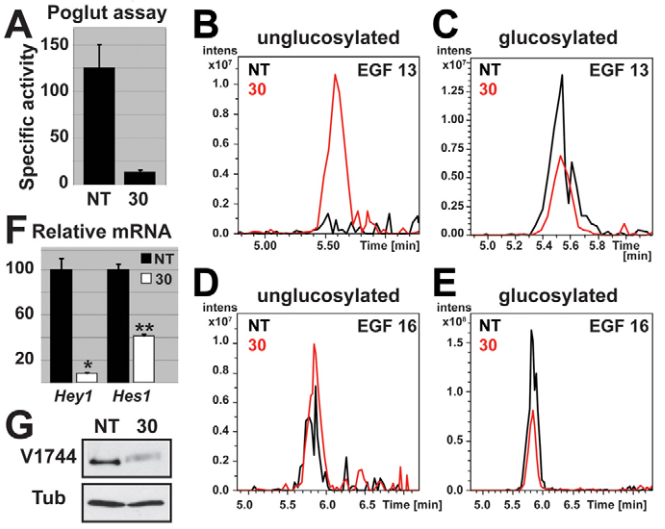


**Fig. 6. Rumi knockdown results in decreased Notch signaling and reduced Notch *O*-glucosylation in C2C12 cells.** (**A**) Poglut assays show a ~90% decrease in the enzymatic activity of C2C12-30 cells compared with C2C12-NT cells. Data are mean±s.e.m. (**B-E**) Rumi knockdown by shRNA-30 results in a dramatic decrease in the levels of *O*-glucosylation of Notch2 EGF repeats as shown by mass spectrometry. (B) The unglucosylated form of the $^{470}$EVNECQSNPCVNNGQCV$^{486}$ peptide from EGF13 is present in the Rumi knockdown sample but not in the control. Underline indicates the *O*-glucosylated serine. (C) The *O*-glucosylated form of this peptide is more abundant in the control than in the Rumi knockdown sample. (D) The unglucosylated form of the $^{585}$DECYSSPCLN$^{594}$ peptide from EGF16 is more abundant in the Rumi knockdown sample than in the control. Underline indicates the *O*-glucosylated serine. (E) The *O*-glucosylated form of this peptide is more abundant in the control than in the Rumi knockdown sample. See Fig. S4 in the supplementary material for MS and MS/MS spectra for B-E. (**F**) qRT-PCR for *Hey1* and *Hes1* on C2C12-30 and C2C12-NT cells. Data are mean±s.e.m. (**G**) Western blot using anti-Val1744 antibody (V1744). α-Tubulin (Tub) was used as loading control.

despite moderate to high level expression of *Kdelc1* and *Kdelc2* in these cells (data not shown). To examine the effects of Rumi knockdown on *O*-glycosylation of Notch EGF repeats, we performed differential mass spectrometry (Acar et al., 2008) on a Myc-6xHis-tagged fragment of the Notch2 extracellular domain harboring EGF13-18 expressed in C2C12-NT and C2C12-30 cells (Fig. 6B-E). The results suggest that the mNotch2 EGF repeats contain an *O*-linked xylose-xylose-glucose trisaccharide (see Fig. S4 in the supplementary material), which is identical to those found on EGF repeats from mNotch1 (Moloney et al., 2000; Bakker et al., 2009; Whitworth et al., 2010). A significant decrease in the *O*-glucosylated form and a corresponding increase in the unglucosylated form of peptides from EGF 13, 16, 17 and 18 were observed in samples from C2C12-30 cells compared with those in C2C12-NT cells (Fig. 6B-E and not shown). These data demonstrate that reduction in mammalian Rumi causes a reduction in the levels of *O*-glucosylation of Notch EGF repeats. Of note, a significant amount of the unglucosylated peptide from EGF16 was detected in the control sample (Fig. 6D), strongly suggesting that different Notch EGF repeats show different levels of *O*-glucose occupancy at endogenous levels of Rumi.

qRT-PCR assays for the Notch pathway effectors show a 92% decrease in *Hey1* mRNA and a 59% decrease in *Hes1* mRNA in C2C12-30 cells (Fig. 6F). We also performed western blots on protein extracts from C2C12-30 and C2C12-NT cells with anti-Val1744 – an antibody that specifically recognizes the γ-secretase cleavage product of Notch1 (Huppert et al., 2005). We find a dramatic reduction in the level of activated Notch1 in C2C12-30 cells (Fig. 6G). These data directly link the function of Rumi to the regulation of Notch signaling in C2C12 cells, and strongly suggest that the Poglut activity of Rumi is required for the activation of Notch1 in these cells.

To begin to address the mechanism of loss of Notch signaling in C2C12-30 cells, we asked whether Rumi regulates the surface expression and ligand binding of Notch in these cells. Biotinylation assays indicate that Notch1 reaches the surface of both C2C12-30 and C2C12-NT cells (Fig. 7A). Flow cytometry with an anti-Notch1 antibody confirms this observation but indicates a 20% decrease in the level of Notch1 at the surface of C2C12-30 cells compared with C2C12-NT cells (Fig. 7B). However, this modest decrease in Notch1 surface levels cannot explain the severe decrease in the level of Notch target expression and activated form

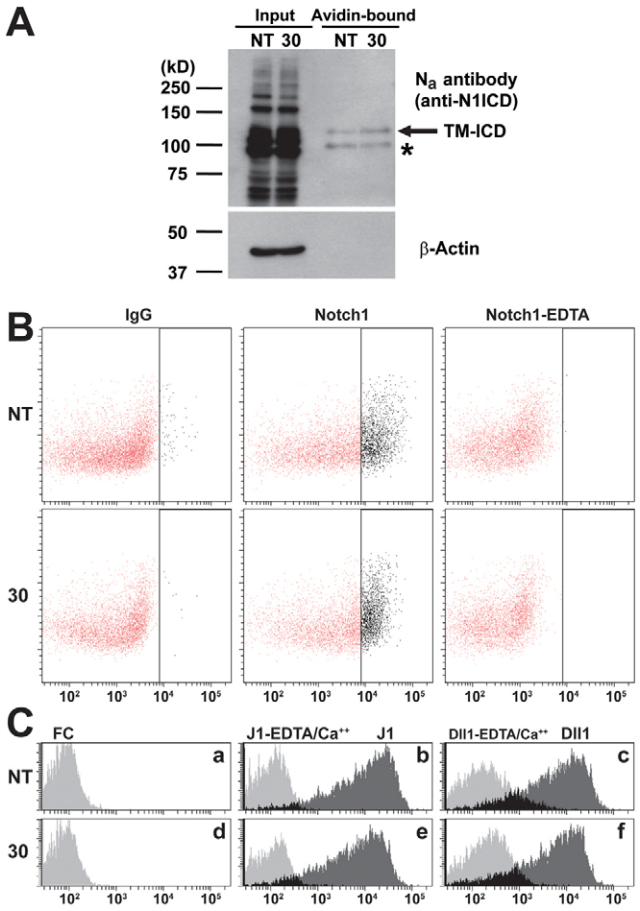


**Fig. 7. Notch ligand binding is not decreased upon Rumi knockdown.** (**A**) Biotinylation assays on C2C12-NT and C2C12-30 cells show that Notch1 is present at the surface of both cell lines, as evidenced by the immunodetection of the N1ICD in the Avidin-bound samples. Data are representative from three independent experiments. β-Actin was used to indicate that intracellular proteins are not present in the Avidin-bound fraction, and also serves as a loading control for the input. TM-ICD indicates migration position of the transmembrane-intracellular fragment of Notch1. Asterisk indicates a non-specific C-terminal truncation of the TM-ICD, which is still exposed extracellularly and can be labeled by biotin. (**B**) Flow cytometry of Notch1 cell surface expression. Surface Notch1 was detected on both C2C12-NT and C2C12-30 cells (black dots to the right of the vertical line in the forward scatter plots). A modest yet significant difference in the mean fluorescence intensities (MFI) between C2C12-NT (MFI: 20580±340) and C2C12-30 (MFI: 16081±147) was observed ($n$=3, $P$=0.0003). Notch1 heterodimer removal by EDTA treatment resulted in negative immunolabeling. (**C**) Flow cytometry of ligand binding. Unlike the Fc negative control (a,d), both C2C12-NT and C2C12-30 cells strongly bind Jag1 (J1) and Delta-like1 (Dll1) (dark-gray histograms in b,c,e,f). No statistically significant difference was observed in their binding ability towards Jag1 ($P$=0.25) or Delta-like1 ($P$=0.92), as determined by comparison of the mean fluorescence intensities: C2C12-NT, J1 (MFI: 15819±435); C2C12-30, J1 (MFI: 17817±1423); C2C12-NT, Dll1 (MFI: 10402±491); C2C12-30, Dll1 (MFI: 10312±660). Incubation with EDTA/$Ca^{++}$ (J1-EDTA/$Ca^{++}$ and Dll1-EDTA/$Ca^{++}$) results in leftward shift of the histograms (light-gray histograms in b,c,e,f), indicating the specificity of the binding assays. Flow cytometry profiles are representative of three independent experiments.

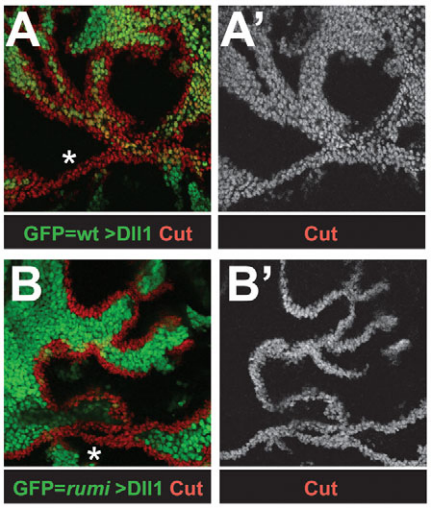


**Fig. 8. Protein *O*-glucosylation is not essential for the function of rat Dll1 in *Drosophila*.** GFP-NLS marks MARCM clones of a wild-type chromosome (A) or the $rumi^{\Delta 26}$ null allele (B) simultaneously expressing rat Dll1. (**A-B′**) Expression of rat Dll1 in *rumi* clones induces a strong expression of the Notch downstream target Cut in neighboring cells outside the clones (B,B′), similar to wild-type clones expressing rat Dll1 (A,A′). In wild-type cells, rat Dll1 does not show a cis-inhibitory effect on *Drosophila* Notch and is able to induce Cut expression in the clones (A,A′), as reported previously (Geffers et al., 2007). However, inside *rumi* clones, induction of Cut by rat Dll1 is abolished, most probably because of the impaired reception of Notch signaling in *rumi* clones. Asterisks in A and B indicate the endogenous wing margin, which expresses Cut independently of the rat Dll1 overexpression.

of Notch1 upon Rumi knockdown. Moreover, flow cytometric analysis of ligand binding indicates that Rumi knockdown in C2C12-30 cells does not decrease the ability of Notch receptors to bind Jag1 and Delta-like1 ligands (Fig. 7C). Altogether, these data strongly suggest that Rumi primarily regulates Notch signaling at a step between ligand binding and S3 cleavage.

In addition to Notch receptors, most canonical ligands in mammals have between one to four Rumi target motifs (see Fig. S5 in the supplementary material and not shown) (Jafar-Nejad et al., 2010). To examine whether *O*-glucosylation is required for the function of mammalian Notch ligands, we performed cross-species transgenic analyses in *Drosophila*, where *rumi* mutations result in a complete loss of Notch signaling at 30°C (Acar et al., 2008). Overexpression of rat Delta-like 1 (Dll1) – with two predicted Rumi target EGF repeats – in *rumi* mutant clones in third instar wing imaginal discs raised at 30°C was able to induce Notch signaling in neighboring cells, as evidenced by the strong induction of the Notch downstream target Cut (Fig. 8A-B′). We performed similar experiments to examine whether the function of Jag1 and Dll3 depends on Rumi, but were not able to reach a conclusion, because these two mammalian ligands did not induce Notch signaling in wild-type or $Rumi^{-/-}$ clones in *Drosophila* using this assay (see Fig. S5 in the supplementary material), in agreement with a previous report on Dll3 (Geffers et al., 2007). These data suggest that *O*-glucosylation by Rumi is not essential for the function of the rat Dll1.

## Rumi regulates Jag1-induced Notch signaling in a dosage-sensitive manner in the mouse liver

To provide further in vivo evidence for the regulation of mouse Notch signaling by Rumi, we sought to determine whether decreasing the level of Rumi affects mouse Notch signaling in a $Jag1^{+/-}$ haploinsufficient background, as these animals are especially sensitive to alterations in the gene dose of other Notch

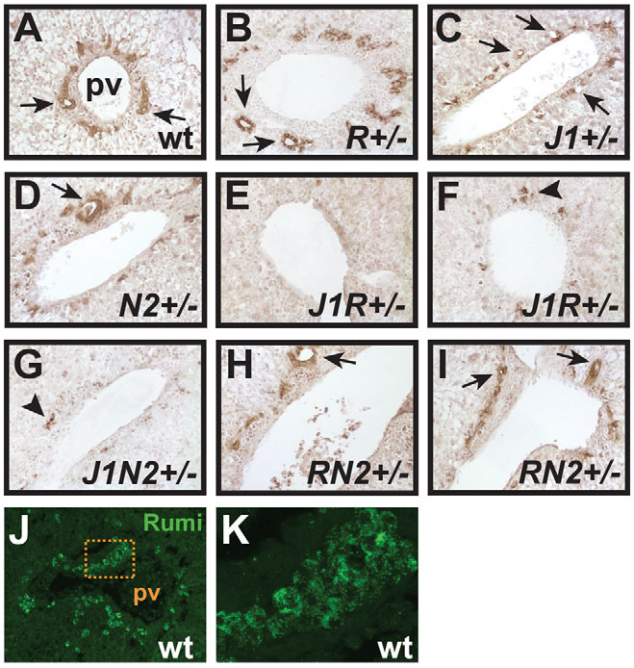


**Fig. 9. Genetic interaction between *Rumi* and *Jag1* in the mouse.** (**A-I**) DBA histochemical staining of biliary cells in P0 livers. Patent bile ducts (arrows) and biliary cells are found around the portal vein (pv) in wild-type (A), *Rumi*$^{+/-}$ (B), *Jag1*$^{dDSL/+}$ (C), *Notch2*$^{del3/+}$ (D) and *Rumi*$^{+/-}$, *Notch2*$^{del3/+}$ (H,I) animals. By contrast, *Jag1*$^{dDSL/+}$, *Rumi*$^{+/-}$ livers show bile duct paucity, with either no biliary cells (E) or a few scattered ones (arrowhead in F), similar to *Jag1*$^{dDSL/+}$, *Notch2*$^{del3/+}$ livers (G). (**J**,**K**) Rumi immunofluorescent stainings of E18.5 liver sections. (K) A high magnification view of the area outlined in J showing the punctate cytoplasmic pattern of Rumi expression in a cluster of cells.

pathway components (Xue et al., 1999; McCright et al., 2001; McCright et al., 2002; Ryan et al., 2008). We crossed the *Rumi*$^{+/-}$ mice to animals heterozygous for the null allele *Jagged1*$^{dDLS}$ (Xue et al., 1999) and analyzed liver sections of P0 animals double heterozygous for the null allele *Jagged1*$^{dDLS}$ (Xue et al., 1999), and our *Rumi* allele and also their control littermates for binding to the *Dolichos biflorus* agglutinin (DBA) – a marker for bile duct epithelial cells (Watanabe et al., 1981). P0 livers of *Rumi*$^{+/-}$ mice showed patent bile ducts and numerous biliary cells around the portal veins, similar to their wild-type littermates and animals heterozygous for *Jagged1*$^{dDSL}$ or the null allele *Notch2*$^{del3}$ (McCright et al., 2006) (Fig. 9A-D). However, all of the five P0 *Jag1*$^{+/-}$, *Rumi*$^{+/-}$ double heterozygous mice analyzed in our studies displayed bile duct paucity and a severe decrease in the number of biliary cells in the periportal regions (Fig. 9E,F). As positive control, we generated P0 animals double heterozygous for *Jagged1*$^{dDSL}$ and the null allele *Notch2*$^{del3}$. These mice also showed bile duct phenotypes comparable with *Jag1*$^{+/-}$, *Notch2*$^{del1/+}$ (hypomorphic) (McCright et al., 2002) and *Jag1*$^{+/-}$, *Rumi*$^{+/-}$ animals (compare Fig. 9G with 9E,F). Of note, P0 animals double heterozygous for *Rumi*$^{-}$ and *Notch2*$^{del3}$ have patent bile ducts in the periportal regions (Fig. 9H,I). Anti-Rumi staining of wild-type E18.5 liver sections shows that some cells in the periportal regions express high levels of Rumi, in agreement with a dose-sensitive role in bile duct morphogenesis (Fig. 9G,K). These observations indicate that Rumi regulates mammalian Notch signaling in vivo, and that Jag1-induced signaling is sensitive to the gene dosage of *Rumi*.

## DISCUSSION

Multiple lines of evidence indicate that, similar to its *Drosophila* homolog, mouse Rumi regulates Notch signaling. Notch signaling negatively regulates the number, length and branching of neurites in Neuro2A cells (Franklin et al., 1999; Mishra-Gorur et al., 2002; Ishikura et al., 2005). Therefore, increased neurite outgrowth and decreased *Hes1* expression upon RNAi-mediated knockdown of Rumi in Neuro2A cells indicate a role for Rumi in the modulation of Notch signaling. In C2C12 cells, Rumi knockdown results in a significant decrease in Poglut activity and impaired Notch1 signaling, as evidenced by reduced levels of activated Notch1 ICD and *Hey1* and *Hes1* mRNA. Last but not least, removing one copy of *Rumi* results in bile duct defects in *Jag1*$^{+/-}$ haploinsufficient animals. Together, these data provide strong evidence that mammalian Notch signaling is modulated by Rumi.

EGF repeats of both Notch1 (Moloney et al., 2000; Bakker et al., 2009; Whitworth et al., 2010) and Notch2 (Fig. 6) are *O*-glucosylated in mammalian cell lines. Despite the co-expression of moderate levels of *Kdelc1* and *Kdelc2* with *Rumi*, we observe a significant decrease in Poglut activity and the level of *O*-glucosylated Notch2 EGF repeats in Rumi knockdown C2C12 cells and a ~50% reduction in Poglut activity in *Rumi*$^{+/-}$ heterozygous livers. These data strongly suggest that of the three soluble ER proteins with a CAP10 domain found in mammals, Rumi is the only one able to add *O*-glucose to Notch proteins. The lack of compensation by KDELC1 and KDELC2 might be because these proteins lack a WXGG motif, which is thought to mediate the binding of clostridial *O*-glucosyltransferases to UDP-glucose (Busch et al., 2000) and is present in fly and mammalian Rumi proteins. Therefore, both in mouse cell lines and in the developing liver, the Notch loss-of-function phenotypes observed upon decreased Rumi levels correlate with decreased Poglut activity. The significant increase in neurite outgrowth observed in *Rumi* knockdown Neuro2A cells can be rescued by overexpression of hRumi but not with an enzymatically inactive mutant version of hRumi. These observations, together with our flow cytometry data and the severe decrease in Notch1 ICD in C2C12-30 cells strongly suggest that addition of *O*-glucose to Notch pathway components regulates mammalian Notch signaling at a step between ligand binding and S3 cleavage of Notch receptors.

Even though *Notch1-4* quadruple knockout phenotypes are not known, comparison of the phenotypes displayed by *Rumi*$^{-/-}$ embryos with those of global regulators of canonical Notch signaling (Oka et al., 1995; Donoviel et al., 1999; Shi and Stanley, 2003) suggests that in addition to the Notch pathway components, other proteins are likely to depend on the function of Rumi during mouse embryonic development. We performed extensive database searches and identified 47 mouse proteins with EGF repeats harboring a consensus *O*-glucosylation motif (see Table S2 in the supplementary material). We found reports on mutant phenotypes for 38 of these targets, but to our knowledge none of these mutants exhibit the combination of phenotypes observed in *Rumi*$^{-/-}$ embryos (see Table S2 in the supplementary material and references therein). It is therefore likely that a combined defect in several targets of Rumi including the Notch pathway components is responsible for the early lethality and the phenotypes observed in *Rumi*$^{-/-}$ embryos.

The dosage-sensitive interaction observed between *Jag1* and *Rumi* strongly suggests that when the level of Jag1 is limiting, optimal Jag1-induced signaling becomes sensitive to the degree of

*O*-glucosylation conferred by Rumi on one or more Notch pathway components. The high-level expression of Rumi in a subset of periportal cells suggests that in this context optimal Notch signaling requires high levels of *O*-glucose occupancy on Notch EGF repeats. Even though Notch2 plays a dominant role in bile duct morphogenesis, analysis of the three dimensional architecture of the intrahepatic bile ducts indicates that, in addition to Notch2, Notch1 and potentially other Notch receptors contribute to bile duct formation in a redundant fashion (Sparks et al., 2010). Accordingly, our observation that newborn $Rumi^{+/-}$, $Notch2^{del3/+}$ animals do not show bile duct phenotypes suggests that decreased glucosylation of several Notch receptors and/or the Jag1 protein itself contributes to the bile duct abnormalities in $Jag1^{+/-}$, $Rumi^{+/-}$ double heterozygous animals. Mutations in *JAG1* are identified in 94% of individuals with Alagille syndrome (Warthen et al., 2006). However, it is not uncommon to find other family members of an affected child with the same point mutation in *JAG1* but with much milder symptoms, strongly suggesting that genetic and/or environmental modifiers play a significant role in the clinical presentation and prognosis of this disease (Li et al., 1997; Emerick et al., 1999). Our data suggest that human *RUMI* (*POGLUT1*) might represent a genetic modifier of *JAG1* phenotypes in individuals with Alagille syndrome.

**Acknowledgements**

We thank Nadia Rana, Yi-Dong Li, Zhengmei Mao, Shinako Kakuda, Eva Zsigmond, Aleksey Domozhirov, Zizhen Wu, Jim Martin, David Haviland and Nathalie Brouard for technical assistance; Pamela Stanley and members of the Jafar-Nejad and Haltiwanger labs for discussions; Rafi Kopan, Bernadette Holdener and Tom Van Lee for comments on the manuscript; and Tom Gridley, Robert Jaekel, Thomas Klein, Pamela Stanley, Rafi Kopan and the Developmental Studies Hybridoma Bank for animals and reagents. We acknowledge support from the NIH (R01GM084135 to H.J.-N. and R01GM061126 to R.S.H.), from The March of Dimes Foundation (Basil O'Connor Starter Scholar Research Award No. 5-FY07-654 and Research Grant No. 1-FY10-362 to H.J.-N.) and from the Mizutani Foundation for Glycoscience (H.T.). Deposited in PMC for release after 12 months.

**Competing interests statement**

The authors declare no competing financial interests.

**Supplementary material**

Supplementary material for this article is available at
http://dev.biologists.org/lookup/suppl/doi:10.1242/dev.060020/-/DC1

**References**

**Acar, M., Jafar-Nejad, H., Takeuchi, H., Rajan, A., Ibrani, D., Rana, N. A., Pan, H., Haltiwanger, R. S. and Bellen, H. J.** (2008). Rumi is a CAP10 domain glycosyltransferase that modifies Notch and is required for Notch signaling. *Cell* **132**, 247-258.

**Bakker, H., Oka, T., Ashikov, A., Yadav, A., Berger, M., Rana, N. A., Bai, X., Jigami, Y., Haltiwanger, R. S., Esko, J. D. et al.** (2009). Functional UDP-xylose transport across the endoplasmic reticulum/Golgi membrane in a Chinese hamster ovary cell mutant defective in UDP-xylose Synthase. *J. Biol. Chem.* **284**, 2576-2583.

**Bischof, J., Maeda, R. K., Hediger, M., Karch, F. and Basler, K.** (2007). An optimized transgenesis system for Drosophila using germ-line-specific phiC31 integrases. *Proc. Natl. Acad. Sci. USA* **104**, 3312-3317.

**Bulman, M. P., Kusumi, K., Frayling, T. M., McKeown, C., Garrett, C., Lander, E. S., Krumlauf, R., Hattersley, A. T., Ellard, S. and Turnpenny, P. D.** (2000). Mutations in the human delta homologue, DLL3, cause axial skeletal defects in spondylocostal dysostosis. *Nat. Genet.* **24**, 438-441.

**Busch, C., Hofmann, F., Gerhard, R. and Aktories, K.** (2000). Involvement of a conserved tryptophan residue in the UDP-glucose binding of large clostridial cytotoxin glycosyltransferases. *J. Biol. Chem.* **275**, 13228-13234.

**Chang, Y. C. and Kwon-Chung, K. J.** (1999). Isolation, characterization, and localization of a capsule-associated gene, CAP10, of Cryptococcus neoformans. *J. Bacteriol.* **181**, 5636-5643.

**Donoviel, D. B., Hadjantonakis, A. K., Ikeda, M., Zheng, H., Hyslop, P. S. and Bernstein, A.** (1999). Mice lacking both presenilin genes exhibit early embryonic patterning defects. *Genes Dev.* **13**, 2801-2810.

**Eldadah, Z. A., Hamosh, A., Biery, N. J., Montgomery, R. A., Duke, M., Elkins, R. and Dietz, H. C.** (2001). Familial tetralogy of Fallot caused by mutation in the jagged1 gene. *Hum. Mol. Genet.* **10**, 163-169.

**Ellisen, L. W., Bird, J., West, D. C., Soreng, A. L., Reynolds, T. C., Smith, S. D. and Sklar, J.** (1991). TAN-1, the human homolog of the Drosophila notch gene, is broken by chromosomal translocations in T lymphoblastic neoplasms. *Cell* **66**, 649-661.

**Emerick, K. M., Rand, E. B., Goldmuntz, E., Krantz, I. D., Spinner, N. B. and Piccoli, D. A.** (1999). Features of Alagille syndrome in 92 patients: frequency and relation to prognosis. *Hepatology* **29**, 822-829.

**Fernandez-Valdivia, R., Jeong, J., Mukherjee, A., Soyal, S. M., Li, J., Ying, Y., Demayo, F. J. and Lydon, J. P.** (2010). A mouse model to dissect progesterone signaling in the female reproductive tract and mammary gland. *Genesis* **48**, 106-113.

**Fortini, M. E.** (2009). Notch signaling: the core pathway and its posttranslational regulation. *Dev. Cell* **16**, 633-647.

**Franklin, J. L., Berechid, B. E., Cutting, F. B., Presente, A., Chambers, C. B., Foltz, D. R., Ferreira, A. and Nye, J. S.** (1999). Autonomous and non-autonomous regulation of mammalian neurite development by Notch1 and Delta1. *Curr. Biol.* **9**, 1448-1457.

**Garg, V., Muth, A. N., Ransom, J. F., Schluterman, M. K., Barnes, R., King, I. N., Grossfeld, P. D. and Srivastava, D.** (2005). Mutations in NOTCH1 cause aortic valve disease. *Nature* **437**, 270-274.

**Geffers, I., Serth, K., Chapman, G., Jaekel, R., Schuster-Gossler, K., Cordes, R., Sparrow, D. B., Kremmer, E., Dunwoodie, S. L., Klein, T. et al.** (2007). Divergent functions and distinct localization of the Notch ligands DLL1 and DLL3 in vivo. *J. Cell Biol.* **178**, 465-476.

**Hansen, G. M., Markesich, D. C., Burnett, M. B., Zhu, Q., Dionne, K. M., Richter, L. J., Finnell, R. H., Sands, A. T., Zambrowicz, B. P. and Abuin, A.** (2008). Large-scale gene trapping in C57BL/6N mouse embryonic stem cells. *Genome Res.* **18**, 1670-1679.

**Harris, R. J. and Spellman, M. W.** (1993). O-linked fucose and other post-translational modifications unique to EGF modules. *Glycobiology* **3**, 219-224.

**Hase, S., Kawabata, S., Nishimura, H., Takeya, H., Sueyoshi, T., Miyata, T., Iwanaga, S., Takao, T., Shimonishi, Y. and Ikenaka, T.** (1988). A new trisaccharide sugar chain linked to a serine residue in bovine blood coagulation factors VII and IX. *J. Biochem. (Tokyo)* **104**, 867-868.

**Hicks, C., Johnston, S. H., diSibio, G., Collazo, A., Vogt, T. F. and Weinmaster, G.** (2000). Fringe differentially modulates Jagged1 and Delta1 signalling through Notch1 and Notch2. *Nat. Cell Biol.* **2**, 515-520.

**Huppert, S. S., Ilagan, M. X., De Strooper, B. and Kopan, R.** (2005). Analysis of Notch function in presomitic mesoderm suggests a gamma-secretase-independent role for presenilins in somite differentiation. *Dev. Cell* **8**, 677-688.

**Ishikura, N., Clever, J. L., Bouzamondo-Bernstein, E., Samayoa, E., Prusiner, S. B., Huang, E. J. and DeArmond, S. J.** (2005). Notch-1 activation and dendritic atrophy in prion disease. *Proc. Natl. Acad. Sci. USA* **102**, 886-891.

**Jafar-Nejad, H., Leonardi, J. and Fernandez-Valdivia, R.** (2010). Role of glycans and glycosyltransferases in the regulation of Notch signaling. *Glycobiology* **20**, 931-949.

**Joutel, A., Corpechot, C., Ducros, A., Vahedi, K., Chabriat, H., Mouton, P., Alamowitch, S., Domenga, V., Cecillion, M., Marechal, E. et al.** (1996). Notch3 mutations in CADASIL, a hereditary adult-onset condition causing stroke and dementia. *Nature* **383**, 707-710.

**Kimata, Y., Ooboki, K., Nomura-Furuwatari, C., Hosoda, A., Tsuru, A. and Kohno, K.** (2000). Identification of a novel mammalian endoplasmic reticulum-resident KDEL protein using an EST database motif search. *Gene* **261**, 321-327.

**Kopan, R. and Ilagan, M. X.** (2009). The canonical Notch signaling pathway: unfolding the activation mechanism. *Cell* **137**, 216-233.

**Krebs, L. T., Xue, Y., Norton, C. R., Shutter, J. R., Maguire, M., Sundberg, J. P., Gallahan, D., Closson, V., Kitajewski, J., Callahan, R. et al.** (2000). Notch signaling is essential for vascular morphogenesis in mice. *Genes Dev.* **14**, 1343-1352.

**Kuhnert, F., Campagnolo, L., Xiong, J. W., Lemons, D., Fitch, M. J., Zou, Z., Kiosses, W. B., Gardner, H. and Stuhlmann, H.** (2005). Dosage-dependent requirement for mouse Vezf1 in vascular system development. *Dev. Biol.* **283**, 140-156.

**Lee, S. Y., Kumano, K., Nakazaki, K., Sanada, M., Matsumoto, A., Yamamoto, G., Nannya, Y., Suzuki, R., Ota, S., Ota, Y. et al.** (2009). Gain-of-function mutations and copy number increases of Notch2 in diffuse large B-cell lymphoma. *Cancer Sci.* **100**, 920-926.

**Lee, T. and Luo, L.** (2001). Mosaic analysis with a repressible cell marker (MARCM) for Drosophila neural development. *Trends Neurosci.* **24**, 251-254.

**Leonhard-Melief, C. and Haltiwanger, R. S.** (2010). O-fucosylation of thrombospondin type 1 repeats. *Methods Enzymol.* **480**, 401-416.

**Li, L., Krantz, I. D., Deng, Y., Genin, A., Banta, A. B., Collins, C. C., Qi, M., Trask, B. J., Kuo, W. L., Cochran, J. et al.** (1997). Alagille syndrome is caused by mutations in human Jagged1, which encodes a ligand for Notch1. *Nat. Genet.* **16**, 243-251.

**Lu, F. M. and Lux, S. E.** (1996). Constitutively active human Notch1 binds to the transcription factor CBF1 and stimulates transcription through a promoter

containing a CBF1-responsive element. *Proc. Natl. Acad. Sci. USA* **93**, 5663-5667.
**Matsuura, A., Ito, M., Sakaidani, Y., Kondo, T., Murakami, K., Furukawa, K., Nadano, D., Matsuda, T. and Okajima, T.** (2008). O-linked N-acetylglucosamine is present on the extracellular domain of notch receptors. *J. Biol. Chem.* **283**, 35486-35495.
**McCright, B., Gao, X., Shen, L., Lozier, J., Lan, Y., Maguire, M., Herzlinger, D., Weinmaster, G., Jiang, R. and Gridley, T.** (2001). Defects in development of the kidney, heart and eye vasculature in mice homozygous for a hypomorphic Notch2 mutation. *Development* **128**, 491-502.
**McCright, B., Lozier, J. and Gridley, T.** (2002). A mouse model of Alagille syndrome: Notch2 as a genetic modifier of Jag1 haploinsufficiency. *Development* **129**, 1075-1082.
**McCright, B., Lozier, J. and Gridley, T.** (2006). Generation of new Notch2 mutant alleles. *Genesis* **44**, 29-33.
**Mishra-Gorur, K., Rand, M. D., Perez-Villamil, B. and Artavanis-Tsakonas, S.** (2002). Down-regulation of Delta by proteolytic processing. *J. Cell Biol.* **159**, 313-324.
**Moffat, J., Grueneberg, D. A., Yang, X., Kim, S. Y., Kloepfer, A. M., Hinkle, G., Piqani, B., Eisenhaure, T. M., Luo, B., Grenier, J. K. et al.** (2006). A lentiviral RNAi library for human and mouse genes applied to an arrayed viral high-content screen. *Cell* **124**, 1283-1298.
**Moloney, D. J., Shair, L. H., Lu, F. M., Xia, J., Locke, R., Matta, K. L. and Haltiwanger, R. S.** (2000). Mammalian Notch1 is modified with two unusual forms of O-linked glycosylation found on epidermal growth factor-like modules. *J. Biol. Chem.* **275**, 9604-9611.
**Mumm, J. S., Schroeter, E. H., Saxena, M. T., Griesemer, A., Tian, X., Pan, D. J., Ray, W. J. and Kopan, R.** (2000). A ligand-induced extracellular cleavage regulates gamma-secretase-like proteolytic activation of Notch1. *Mol. Cell* **5**, 197-206.
**Nita-Lazar, A. and Haltiwanger, R. S.** (2006). Methods for analysis of O-linked modifications on epidermal growth factor-like and thrombospondin type 1 repeats. *Methods Enzymol.* **417**, 93-111.
**Oda, T., Elkahloun, A. G., Pike, B. L., Okajima, K., Krantz, I. D., Genin, A., Piccoli, D. A., Meltzer, P. S., Spinner, N. B., Collins, F. S. et al.** (1997). Mutations in the human Jagged1 gene are responsible for Alagille syndrome. *Nat. Genet.* **16**, 235-242.
**Oka, C., Nakano, T., Wakeham, A., de la Pompa, J. L., Mori, C., Sakai, T., Okazaki, S., Kawaichi, M., Shiota, K., Mak, T. W. et al.** (1995). Disruption of the mouse RBP-J kappa gene results in early embryonic death. *Development* **121**, 3291-3301.
**Okajima, T. and Irvine, K. D.** (2002). Regulation of notch signaling by o-linked fucose. *Cell* **111**, 893-904.
**Rampal, R., Arboleda-Velasquez, J. F., Nita-Lazar, A., Kosik, K. S. and Haltiwanger, R. S.** (2005). Highly conserved O-fucose sites have distinct effects on Notch1 function. *J. Biol. Chem.* **280**, 32133-32140.
**Roca, C. and Adams, R. H.** (2007). Regulation of vascular morphogenesis by Notch signaling. *Genes Dev.* **21**, 2511-2524.
**Ryan, M. J., Bales, C., Nelson, A., Gonzalez, D. M., Underkoffler, L., Segalov, M., Wilson-Rawls, J., Cole, S. E., Moran, J. L., Russo, P. et al.** (2008). Bile duct proliferation in Jag1/fringe heterozygous mice identifies candidate modifiers of the Alagille syndrome hepatic phenotype. *Hepatology* **48**, 1989-1997.
**Sasamura, T., Sasaki, N., Miyashita, F., Nakao, S., Ishikawa, H. O., Ito, M., Kitagawa, M., Harigaya, K., Spana, E., Bilder, D. et al.** (2003). neurotic, a novel maternal neurogenic gene, encodes an O-fucosyltransferase that is essential for Notch-Delta interactions. *Development* **130**, 4785-4795.
**Shao, L., Luo, Y., Moloney, D. J. and Haltiwanger, R.** (2002). O-glycosylation of EGF repeats: identification and initial characterization of a UDP-glucose: protein O-glucosyltransferase. *Glycobiology* **12**, 763-770.
**Shi, S. and Stanley, P.** (2003). Protein O-fucosyltransferase 1 is an essential component of Notch signaling pathways. *Proc. Natl. Acad. Sci. USA* **100**, 5234-5239.
**Sparks, E. E., Huppert, K. A., Brown, M. A., Washington, M. K. and Huppert, S. S.** (2010). Notch signaling regulates formation of the three-dimensional architecture of intrahepatic bile ducts in mice. *Hepatology* **51**, 1391-1400.
**Stahl, M., Uemura, K., Ge, C., Shi, S., Tashima, Y. and Stanley, P.** (2008). Roles of Pofut1 and O-fucose in mammalian Notch signaling. *J. Biol. Chem.* **283**, 13638-13651.
**Teng, Y., Liu, Q., Ma, J., Liu, F., Han, Z., Wang, Y. and Wang, W.** (2006). Cloning, expression and characterization of a novel human CAP10-like gene hCLP46 from CD34(+) stem/progenitor cells. *Gene* **371**, 7-15.
**Venken, K. J., He, Y., Hoskins, R. A. and Bellen, H. J.** (2006). P[acman]: a BAC transgenic platform for targeted insertion of large DNA fragments in D. melanogaster. *Science* **314**, 1747-1751.
**Warthen, D. M., Moore, E. C., Kamath, B. M., Morrissette, J. J., Sanchez, P., Piccoli, D. A., Krantz, I. D. and Spinner, N. B.** (2006). Jagged1 (JAG1) mutations in Alagille syndrome: increasing the mutation detection rate. *Hum. Mutat.* **27**, 436-443.
**Watanabe, M., Muramatsu, T., Shirane, H. and Ugai, K.** (1981). Discrete distribution of binding sites for Dolichos biflorus agglutinin (DBA) and for peanut agglutinin (PNA) in mouse organ tissues. *J. Histochem. Cytochem.* **29**, 779-780.
**Whitworth, G. E., Zandberg, W. F., Clark, T. and Vocadlo, D. J.** (2010). Mammalian Notch is modified by D-Xyl-{alpha}1-3-D-Xyl-{alpha}1-3-D-Glc-{beta}1-O-Ser: implementation of a method to study O-glucosylation. *Glycobiology* **20**, 287-299.
**Xue, Y., Gao, X., Lindsell, C. E., Norton, C. R., Chang, B., Hicks, C., Gendron-Maguire, M., Rand, E. B., Weinmaster, G. and Gridley, T.** (1999). Embryonic lethality and vascular defects in mice lacking the Notch ligand Jagged1. *Hum. Mol. Genet.* **8**, 723-730.
**Yang, L. T., Nichols, J. T., Yao, C., Manilay, J. O., Robey, E. A. and Weinmaster, G.** (2005). Fringe glycosyltransferases differentially modulate Notch1 proteolysis induced by Delta1 and Jagged1. *Mol. Biol. Cell* **16**, 927-942.